RESEARCH

Apparent activation energy of mineral in open pit mine based upon the evolution of active functional groups

Shipng Lu[1] · Jingyu Zhao[1,2] · Jiajia Song[1] · Jiaming Chang[1] · Chi-Min Shu[3]

Abstract

This study aimed to investigate the mechanism of mineral spontaneous combustion in an open pit. On the study of coal and mineral mixture in open pit mines, as well as through the specific surface area and Search Engine Marketing (SEM) experiments, the specific surface area and aperture characteristics of distribution of open pit coal sample and pit mineral mixture samples were analyzed. Thermal analysis experiments were used to divide the oxidation process was divided into three stages, and the thermal behavior characteristics of experimental samples were characterized. On the basis of the stage division, we explored the transfer law of the key active functional groups of the experimental samples. The apparent activation energy calculation of the key active groups, performed by combining the Achar differential method with the Coats–Redfern integral method, microstructural and oxidation kinetic properties were revealed. The resulted showed that the mixed sample had high ash, the fixed carbon content was reduced, the specific surface area was far lower than the raw coal, the large aperture distribution was slightly higher than the medium hole, the micropore was exceptionally low, the gas adsorption capacity was weaker than the raw coal, the pit coal sample had the exceedingly more active functional groups, easy to react with oxygen, more likely to occur naturally, and its harm was relatively large. The mixed sample contained the highest C–O–C functional group absorbance. The functional groups were mainly influenced by the self-OH content, alkyl side chain, and fatty hydrocarbon in the sample. The main functional groups of the four-like mixture had the highest apparent activation energy, and the two reactions were higher in the low-temperature oxidation phase.

Keywords Specific surface area · Aperture distribution characteristics · Thermal behavior characteristics · Oxidation kinetic properties · Gas adsorption capacity

1 Introduction

Forty percent of the world's coal mine production is the use of open pit mining. As a big country in coal demand, China also has considerable number of open pit coal mines, and the country continues to vigorously promote the improvement of coal mine production capacity. Compared with underground mining, the productivity of open pit mining can reach up to 3 to 5 times that of underground mining. However, open pit mines usually continue to expand, and the continuous increase of pit minerals leads to an increase in the risk of coal spontaneous combustion (CSC) (Cao et al. 2020; Tang 2020; Tang et al. 2020). CSC is a major problem in coal mine safety production (Deng et al. 2015; Liang et al. 2023; Zhao et al. 2022). In the initial stage of CSC, water evaporation and gas desorption will occur, which cause the gradual increase of coal sample surface temperature, thus prompting the oxygen molecule to react deeply with coal through the coal crack, and involving the cleavage of chemical bonds of active functional groups in coal (Aich et al. 2019; Zhang et al. 2018; Zeng and Li 2022). This heat shows action on coal, resulting in the CSC phenomenon. At the same time, the process of coal mining will yield oil shale coal gangue and other wastes, increasing the loss caused by CSC (Chabukdhara and Singh 2016; Ju et al. 2019; Zhang

✉ Jingyu Zhao
   zhaojingyu2014@126.com

[1] School of Safety Science and Engineering, Xi'an University of Science and Technology, Xi'an 710054, China

[2] Shaanxi Industrial Process Safety and Emergency Rescue Engineering Technology Research Center, Xi'an 710054, Shaanxi, China

[3] Department of Safety, Health, and Environmental Engineering, National Yunlin University of Science and Technology, Douliou 64002, Yunlin, Taiwan

et al. 2022). To forestall accidents, it is necessary to fully explore the thermal characteristic parameters of minerals in coal mines.

The existing studies mainly focus on the dynamics of kerosene mother shale and coal gangue. Through Search Engine Marketing (SEM) and X-Ray Diffraction (XRD) tests, the mineral evolution process in the pyrolysis process of oil shale was analyzed and it was found that with the increase of organic matter, the number and area of the oil shale increased, which is conducive to the in-situ development of oil shale (Huang et al. 2023; Liu et al. 2023; Zhai et al. 2023). DSC experiment can study the heat transfer process of oil shale and 500 °C semi-coke. During the combustion of oil shale, four peaks are the heat transfer peaks (30–300 °C), coke combustion (300 °C), carbonate decomposition (700–800 °C) and the volatile organic matter and the heat transfer peak of coke and carbonate. The basic characteristics of oil shale and its pyrolysis products were assessed, and the relative strength of the methyl functional groups in raw semi-coke and residual ore decreased with the pyrolysis. The aliphatic carbon chain is more likely to cleave, and the carbon–oxygen double bond structure is not easy to decompose, and it is more likely to occur in shale oil (Alexander et al. 2023; Jiang et al. 2023; Jin et al. 2023). Using thermal mass-Fourier transform infrared spectroscopy of typical pyrolysis oil shale, the oil shale pyrolysis process can be divided into four stages. Pyrolysis reaction and volatile release mainly occur in the second stage. The more fat hydrocarbon content, the more methane released in the process of pyrolysis, and the formation of methane is by a desorption process with the results of four chemical reactions (Onifade and Genc 2019; Wang et al. 2023; Zheng et al. 2023). The mixed combustion characteristics of biomass and gangue were studied, and the maximum combustion ratio of gangue and 200 °C baking products was obtained (Zhu et al. 2020).

To sum up, numerous scholars have only selected a single product as the research object in the study of pit minerals, analyzed the change law of functional groups, and rarely studied the change of spontaneous combustion characteristic parameters after the mixing of various minerals. Therefore, in this paper, the raw coal and raw coal shale mixed oil shale and gangue samples were selected as the research object. Microscopic characteristics were investigated by specific surface area and SEM experiments, through physical and chemical adsorption by differential scanning calorimetry (DSC) and in-situ infrared technology, the functional group of the two samples was scrutinized in different oxidation stages with temperature. The apparent activation energy of functional groups in different oxidation stages was calculated by Achar differential method and Coats-Redfern integration method, providing theoretical basis for accurate determination of mineral spontaneous combustion state and

expeditious working as adoption of reasonable corresponding measures.

2 Experimental

2.1 Coal sample

Raw coal, oil shale, and coal gangue were collected from the open pit mine as experimental samples, and the selected coal samples of the open pit mine were long-flame coal. The experimental subjects were divided into two groups, one group was raw coal, the other group was the mixed sample made of raw coal, oil shales, redistilled oil shale and coal gangue according to the ratio of 1:1:1:1. The collected coal samples were prepared for crushing, screenings, and sealing. To forestall the oxidation of the coal with oxygen on the coal surface and affect the test results, the middle part of the coal samples was selected as the test sample, and the coal samples of 80–120 mesh were screened for the experiment.

The industrial analysis and elemental analysis experimental results are listed in Fig. 1. Raw coal with 5% moisture, which belongs to low moisture coal, low ash, high volatile, indicated coal sample's flammable high calorific value.

2.2 Specific surface area and microscopic pore test

The specific surface area test used Autosorb-iq-c automatic physical chemical adsorption analyzer, sample particle size of 80–120 mesh; the experiment was conducted at 10 °C below room temperature, and heating rate of 5 °C/min. The experimental atmosphere was nitrogen, and temperature at −196 °C (nitrogen critical point, 77 K). The microscopic pore testing was performed with a German-Zeiss-SIGMA HD scanning electron microscope with sample particle size 80–120 mesh and dried in experimental settings 70,000, 50,000, 20,000, and 10,000 four magnifications.

2.3 Differential scanning calorimetry test

The TA-SDTQ600 thermal analyzer with sample size 80–120 mesh, mass 2 mg, heating rate 10 °C/min, 79% nitrogen + 21% oxygen, from room temperature to, 1000 °C, was used.

2.4 In-situ infrared test

Using the INVENIO type Fourier transform infrared spectrometer of Bruker and in-situ infrared of Specac Selector TM, the sample of 80–120 was 1 mg.

(a) Results of the proximate analysis experiments

(b) Elemental analysis of the experimental results
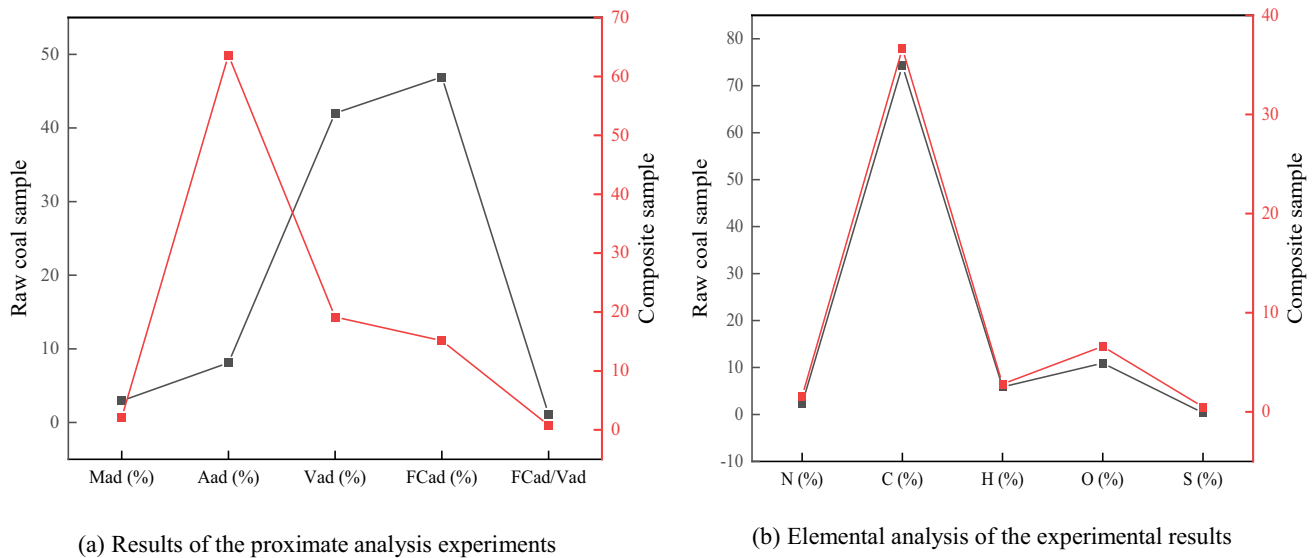
Fig. 1 Results of the proximate analysis experiments and elemental analysis

3 Experimental results and analysis

3.1 Analysis of mineral surface area and microscopic pore of pit

3.1.1 Mineral-specific surface area analysis

For the tested adsorption curve, the BET (Brunauer, Emmett, and Teller) theoretical method was used to calculate the specific surface area of the BET equation as shown in Eq. (1):

$$\frac{p}{Q \cdot (p_0 - p)} = \frac{1}{Q_m \cdot C} + \frac{C - 1}{Q_m \cdot C} \cdot \frac{p}{p_0} \tag{1}$$

In Eq. (1), p is nitrogen fractional pressure, mmHg; p_0 is the saturated vapor pressure of the lower nitrogen gas, mmHg; Q is the amount of nitrogen actually adsorbed on the surface of the experimental sample, cm^3/g; Q_m is the nitrogen saturation of the experimental sample, cm^3/g; C is the constant related to the adsorption capacity. Equation (2) can be obtained from dividing the left and bottom of the equation by P_0:

$$\frac{p/p_0}{Q \cdot (1 - p/p_0)} = \frac{1}{Q_m \cdot C} + \frac{C - 1}{Q_m \cdot C} \cdot \frac{p}{p_0} \tag{2}$$

According to the linear relationship of $(p/p_0)[Q(1 - p/p_0)]$ and p/p_0, the slope and intercept are obtained, the Q_m is solved, and then the specific surface area is determined based upon the area occupied by a single nitrogen gas molecule on the surface. The calculation curve of the specific surface area of the two samples is shown in Fig. 2. The calculated specific surface area of raw coal was 39.38 m^2/g, and the mixed surface area of the composite samples was 4.46 m^2/g.

Overall, the raw coal surface area was larger, to 39.38 m^2/g. At room temperature and pressure, and oxygen coal composite reaction transverse comparison can be found. According to the specific surface area from small to large arrangement for four mixed raw coal, shale's surface area decreased, after oil distillation. Because of the volatile materials in the process of distillation, particle pore structure changed, leading to composite specific surface area being less than the raw coal.

3.1.2 The aperture analysis

There were various classification criteria for pore structures, in which IUPAC tissue is divided into three categories according to the size of pore size range and solid gas, micropores (< 2 nm) mesoporous (2–50 nm), and large pores (> 50 nm). The less the content of large pores and medium pores, the tighter the structure, and the easier it is to react with oxygen at room temperature. According to Table 1, the majority of coal samples were mesoporous, the majority of rock samples were large pores, and the content of micropores in all the samples was extremely small, indicating that the molecular structure of these two samples was unstable, so oxidation and adsorption were more likely under normal temperature ventilation onditions (Fig. 3).

(a) Raw coal sample
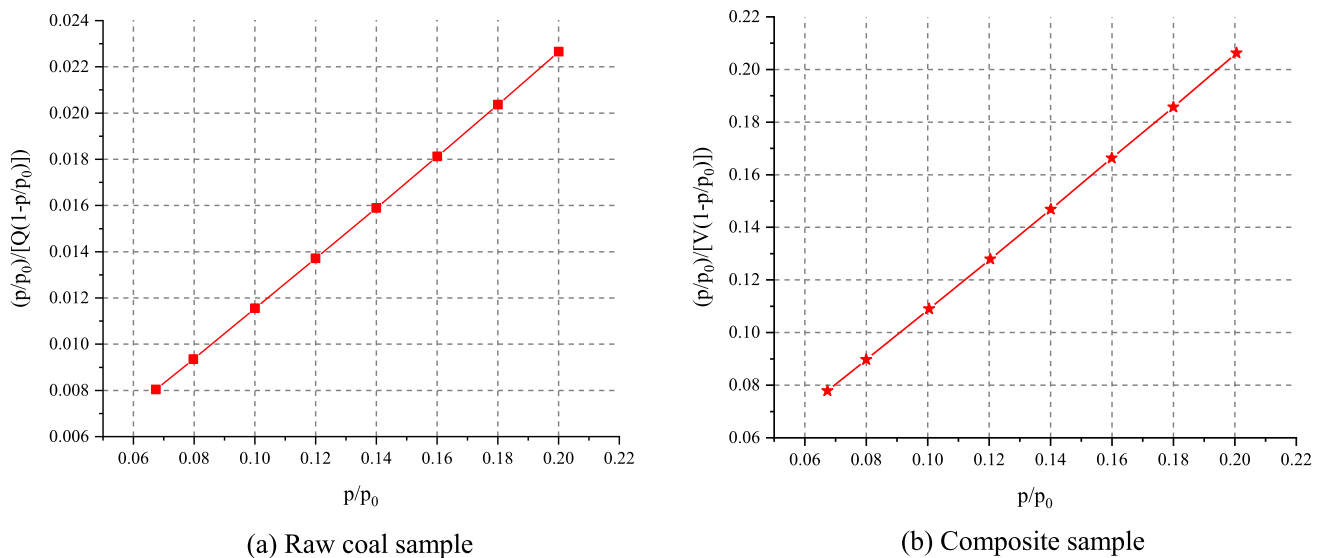
(b) Composite sample

Fig. 2 Specific surface area measured by multi-point BET method for **a** Raw coal and **b** Composite

Table 1 Pore size distribution for raw coal and composite samples

Coal sample	Micropore (%)	Mesoporous pore (%)	Macropore (%)
Raw coal sample	0.62	56.15	43.23
Composite sample	0.22	40.43	59.35
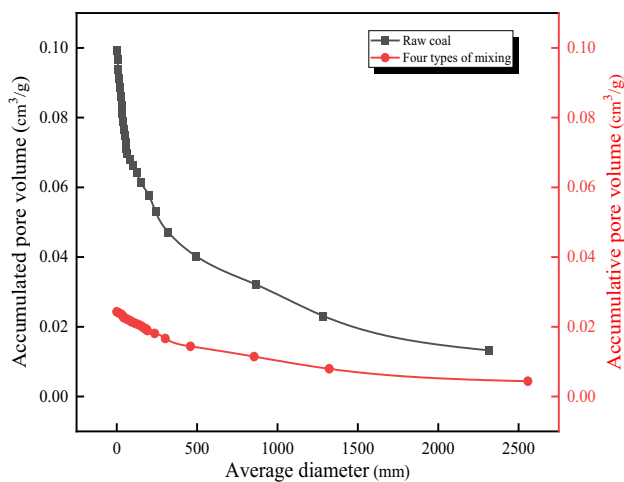
Fig. 3 Change pattern of the cumulative hole volume of the raw coal and composite samples

3.1.3 Micromorphology analysis

The pore and fissure development of the two samples at different magnifications (raw coal on the left and four mixture on the right) were tested, as shown in Fig. 4.

From the SEM map of the above experiments, it was found that both samples had different numbers of stomatal structures at different magnifications. From the SEM scanning image of the raw coal sample, we can see that the raw coal sample was completely flat, and a small amount of clay minerals and coal debris accumulation appeared. From the SEM scanning image of composite samples, it can be observed that the sample had the structural characteristics of each sample at the same time, such as the large amount of clay ore on the surface of coal silk-carbon structure oil shale. As mixed samples' common granular chip debris attached to the sample surface, the surface was rough, uneven with a large number of pores, and silk carbon structure, stripes, silk carbon, leading to a larger surface area. The pores' morphology, a circular ellipsoid and irregular shape, connectivity between pores was poor, and on the surface can clearly be seen part of kaolinite cover. After comparing the raw coal with the composite sample, it can be found that the raw coal has more pore structures. More pore structures increase the oxygen channels of the raw coal, and the surface is covered by some minerals, providing conditions for saving heat.

3.2 Analysis of mineral exothermic characteristics in mines

3.2.1 Analysis of heat flow

Through the observation of experimental data, it can be found that in the DSC curve (Fig. 4), the sample curve with the increase of the temperature possessed the same trend in the initial stage of heat flow being decreased. The above-mentioned was due to water evaporation, that adsorbed heat. During the evaporation process, the heat was produced by
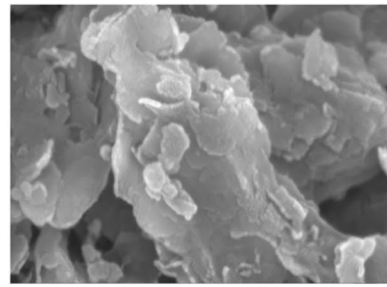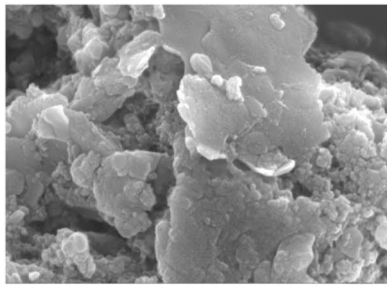
(a) 70,000X magnification
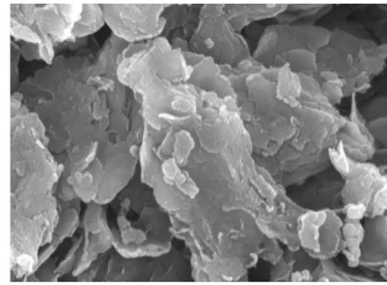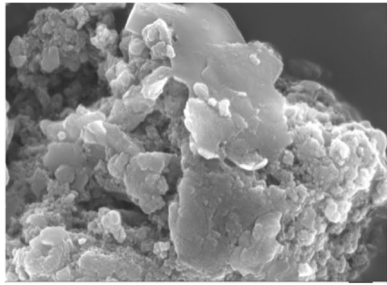
(b) 50,000X magnification
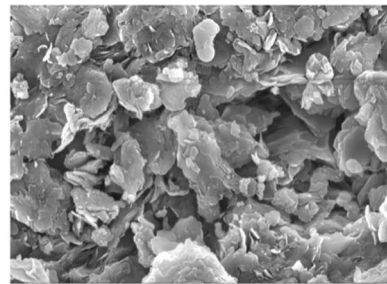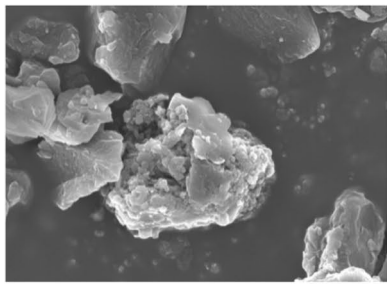
(c) 30,000X magnification
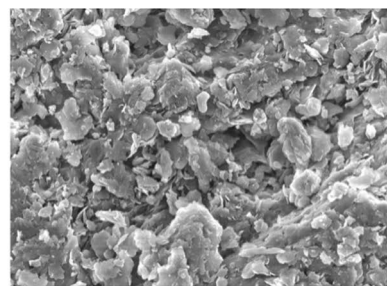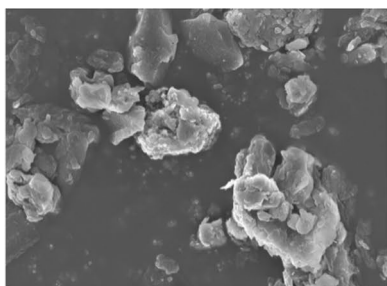
(d) 10,000X magnification

Fig. 4 SEM of raw coal and composite samples

coal's physical adsorption, where heat release was relatively small. Therefore, this stage in the heat adsorption process as the temperature rising DSC curve first rose followed by the downward trend.

During the cold oxidation phase, the DSC curves of the two samples increased with temperature. The heat adsorption effect caused by water evaporation under low-temperature oxidation conditions was weakened, and the chemical

adsorption effect was gradually enhanced, with the heat released being greater than the physical adsorption effect. Therefore, the heat flow value began to rise gradually. Meanwhile, this stage was in the process of heat release. In the rapid heating phase, two samples DSC curve increased with temperature until the peak heat flow, then the heat flow curve commenced to drop. This phenomenon was ascribed to the fact that the sample contained a variety of functional groups. The high activity functional group first reacted with oxygen, then released an immense amount of gas, and finally the low activity functional group in the process of oxidation was gradually activated to participate in the reaction. In the high-temperature combustion stage, the DSC curve of the two samples decreased with the temperature, and then rose to the second peak heat flow. The peak heat flow was between 462 and 478 °C. In addition, the heat flow value started to decrease after reaching the peak. This was because with the rising temperature, there was not only a pyrolysis reaction inside the sample, but also an oxidation combustion reaction. A large number of unstable bridge bonds in the sample underwent bond breaking reactions, cracking at high-temperature, and producing a huge number of small molecule structures and pyrolysis products. The process required more energy, adsorbing part of the reaction to release heat, leading to the reduction of DSC curve. However, oxygen quickly occupied the surface of the sample and reacted with a large number of small molecules produced by cracking, releasing an enormous amount of heat, which was constantly greater than the heat adsorption. Here, the DSC curve showed a rising trend until the peak of heat flow was reached.

Overall, when the fixed heating rate of different coal samples was 10 °C/min, the first exothermal peak temperature was aprox. 326 °C. Furthermore, the heat flow value of raw coal samples was greater than the composite sample. When the temperature of the second exothermic peak was roughly 460 °C, the heat flow value of the raw coal sample was greater than the composite sample. It can be observed that the heat flow of the raw coal sample was the highest. The reaction was exothermic, the heat released was larger, and the raw coal was more prone to spontaneous combustion and produced more harmful gases (Fig. 5).

3.2.2 Heat release analysis

The total heat release of raw coal was 4714.40 J/g, and the total heat release of composite sample coal was 1795.63 J/g. The total heat release of the raw coal sample was the largest, indicating that there were relatively more active functional groups in the raw coal sample, which was easy to participate in the oxidation reaction and generated more deleterious gases. The change of heat release of both samples with temperature is shown in Fig. 6.

The heat release of the two samples had the same change pattern with the temperature increase. The heat release of the sample was exceptionally small in the low-temperature oxidation stage. With the increase of coal temperature, the heat release gradually increased in the expeditious heating stage, and the growth rate accelerated, increasing exponentially. The difference between the two curves is in the rapid heating stage. When the sample is in the rapid heating stage, the growth rate of the raw coal heat release is greater than that of the composite sample, denoting that the raw coal is sensitive to the temperature in this stage, and the oxidation reaction is more intense than that of the composite sample. During the high-temperature combustion phase, the
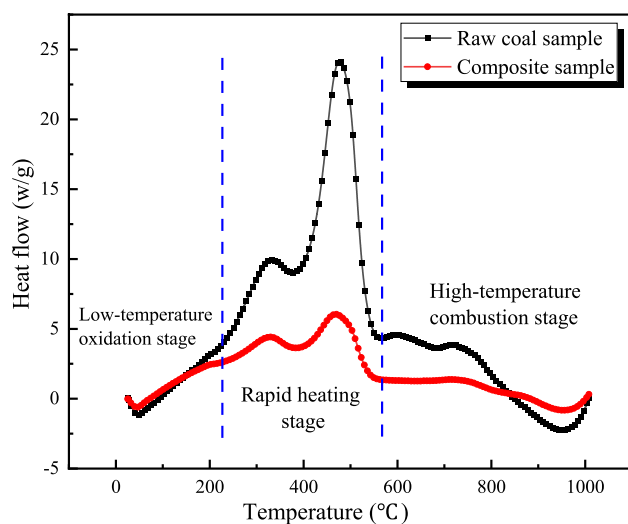
Fig. 5 Mixed heat flow curve of raw coal and composite samples
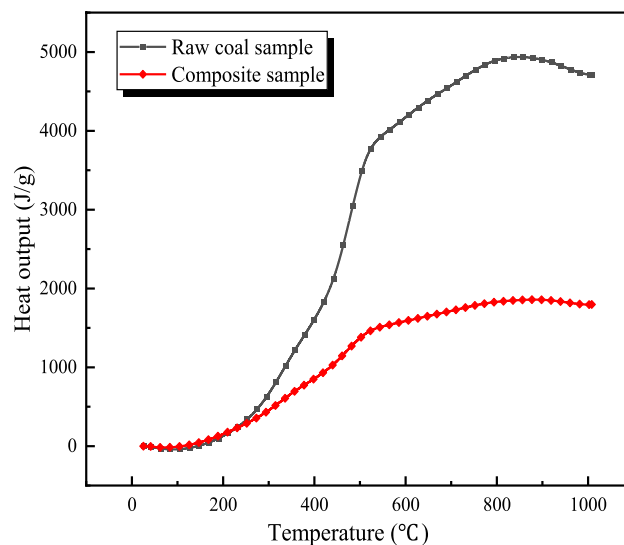
Fig. 6 Plots of heat release of raw coal and composite sample coal with temperature

heat release continued to increase until the peak heat release embarked on to reach plateau. In low-temperature oxidation stage, at the beginning of the reaction, two types of sample heat were less. Even the heat curve showed slightly downward trend, due to water evaporation; it adsorbed heat and release of heat was generated by physical adsorption. Here, exothermic heat was relatively small. Accordingly, in the heat adsorption process, the previous DSC curve tended to be stable and consistent. Then, with the change of temperature, heat started to increase in rapid heating stage. As can be clearly observed, two types of sample heat commenced to present exponential growth. In addition, as the temperature presented the characteristics of highly active functional group that first reacted with oxygen, and then released an immense amount of gas, low active functional group in the process of oxidation gradually activated to participate in the reaction. Therefore, with the rise of temperature, the sample participated in the reaction of active functional quantity, followed by the increase of heat intensity high-temperature combustion stage. For two samples of heat, the temperature continued to increase until the heat peak began to smooth. This was due to a large number of small molecules active agent structure and combustible materials reacting with oxygen, constantly releasing a large amount of heat, and yielding an enormous amount of gases.

3.3 Infrared spectrum analysis of pit minerals

3.3.1 Infrared spectrogram analysis

The position and intensity of the infrared adsorption spectrum peak depended on the vibrational form of the groups in the molecule and the influence of the adjacent groups, reflecting the characteristics of the molecular structure. Because of the various vibration modes of various groups, a large number of adsorption peaks appeared in the infrared spectrogram. Four types of adsorption bands of hydroxyaliphatic aromatics and oxygen-containing functional groups were taken as the characteristic peaks of the sample. The structure can be determined only if these characteristic peaks can be identified.

From the infrared spectrum in Fig. 7, there are differences in the absorption peak intensities of different samples, resulting in the functional groups contained in the experimental samples being basically the same, but with varying quantities. The functional group with greater activity during the oxidation process is the hydroxyl group. The inter-molecular association hydroxyl hydrogen bonds, inter-molecular hydroxyl hydrogen bonds, and free hydroxyl groups contained in different coal samples were the existing differences. Both methyl and methylene are present in all experimental samples, and the methyl deformation vibration absorption intensity is high. In addition, the content of methylene is slightly higher than that of methyl, indicating that methylene is more active during the oxidation process. The methyl absorption intensity of the raw coal sample is higher than that of the composite sample. The main active group during the oxidation process is the oxygen-containing functional group, which has a significant impact on the chemical properties of the sample. From Fig. 6, it can be seen that the C–O–C functional groups contained in the composite sample had the highest absorbance, while the residual C–O–C oxygen-containing functional groups in the raw coal sample were relatively low. Because of the fact that the C=C double

(a) Raw coal sample
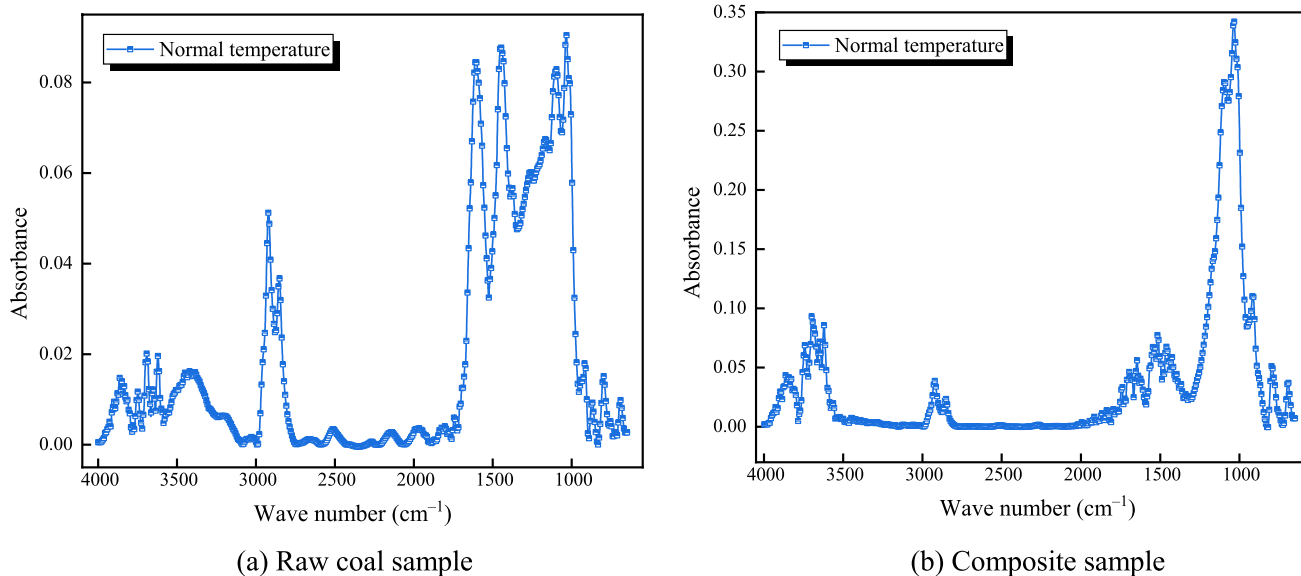
(b) Composite sample

Fig. 7 The IR spectrum of raw coal and composite sample

Table 2 Peak position distribution of active functional groups for raw coal and composite sample

Functional group	Raw coal sample	Composite sample
Free hydroxyl–OH	3690, 3650	3697, 3649
Intramolecular hydrogen bond–OH	3620	3620
Intermolecular association hydrogen bond–OH	3420	3449
Methylene symmetric stretching motion	2852	2852
Methylene asymmetric stretching motion	2920	2923
Methylene shear vibration	1448	1461
Methyl shear vibration	1374	
C=C	1605	1645
C–O	1263	
C–O–C	1032, 1098	1035, 1093
Aromatic hydrocarbons Ar–CH	794, 871	794

bond was the main structure of the aromatic ring and the raw coal had not been oxidized, the double bond structure was stable, the content was high, and the peak intensity was high, resulting in a strong C=C double shoulder absorption spectrum of the raw coal sample. Table 2 summarizes the assigned peaks of different functional groups for different coal samples.

3.3.2 Analysis of functional group transfer law

The curves of different groups with temperature are shown in Figs. 8, 9, 10 and 11. From Fig. 8, it can be seen that hydroxyl groups existed in the oxidation process of each sample. As the temperature increased, the number of hydroxyl groups kept changing, as hydroxyl groups continuously participated in oxidation reactions and were

consumed, and other functional groups reacted with oxygen to generate hydroxyl groups.

During the low-temperature oxidation stage, the intermolecular hydrogen bond strength of inter-molecular hydroxyl groups in raw coal maintains an upward trend. In the composite sample, the strength of inter-molecular hydrogen bonds tends to stabilize while the absorption strength of free hydroxyl groups increases. Meanwhile, some unsaturated hydrocarbons were oxidized to form hydroxyl groups, but the formation rate is greater than the consumption rate. Therefore, there was an upward trend at this stage. In the rapid heating stage, in the composite of the raw coal sample, the light absorption intensity of hydrogen bonds with wave numbers 3690 and 3620 cm^{-1} decreases, while the light absorption density of free hydroxyl groups with a wave length of approximately 3650 cm^{-1} basically increases. In
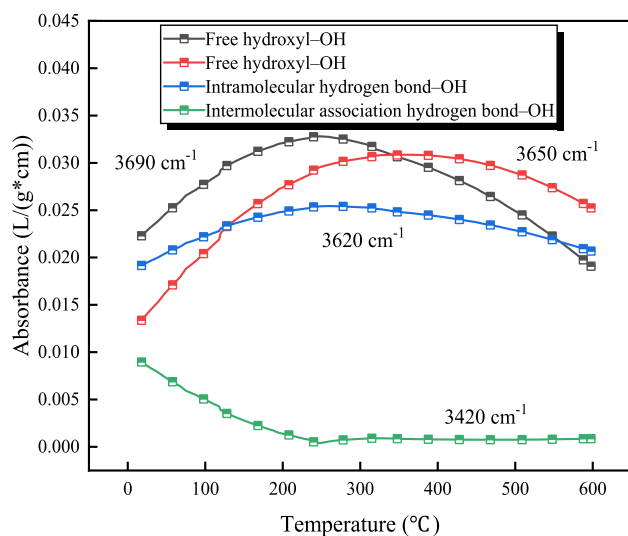
(a) Raw coal sample
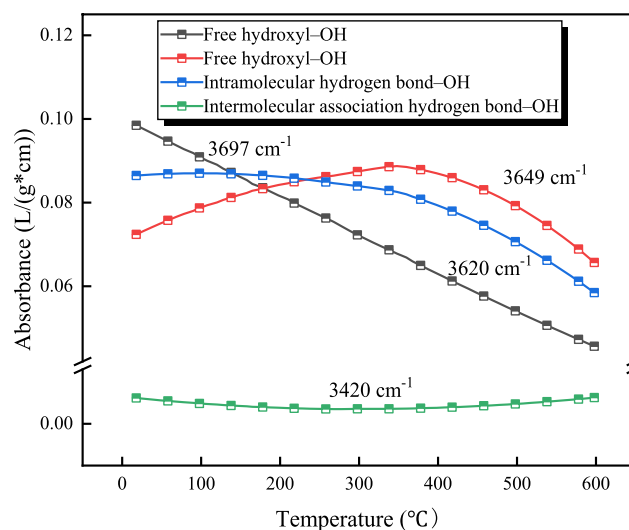
(b) Composite sample

Fig. 8 Curve of the hydroxyl group with temperature for raw coal and composite samples
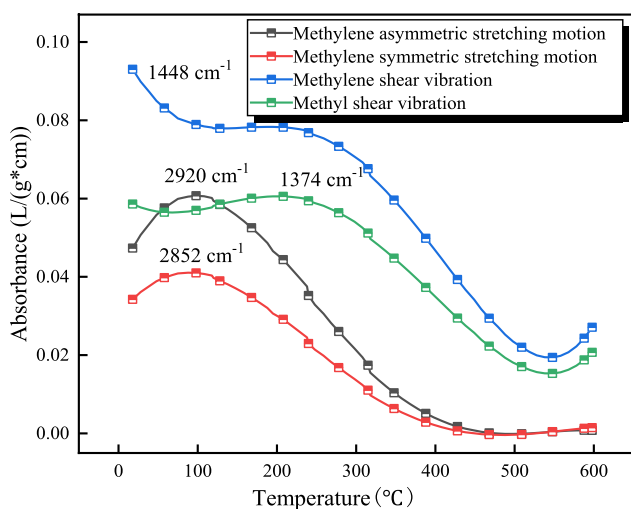
(a) Raw coal sample
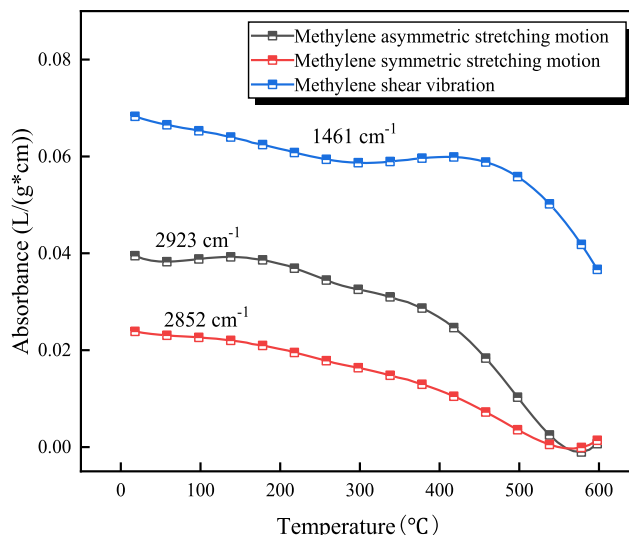
(b) Composite sample

Fig. 9 Curve of fat hydrocarbon with temperature for **a** Raw coal sample and **b** Composite sample
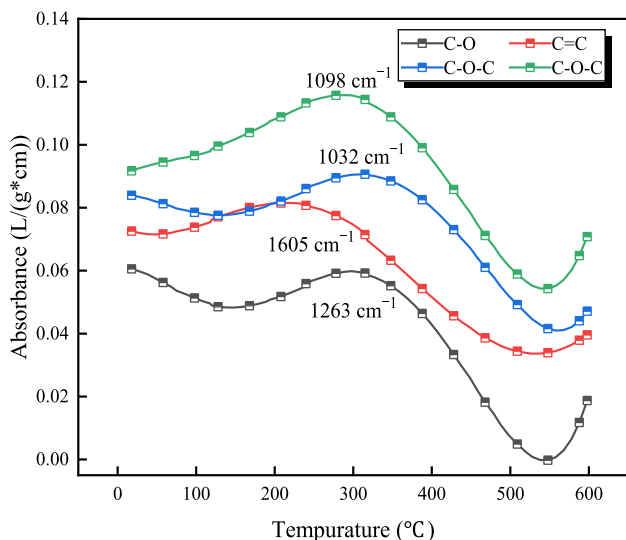
(a) Raw coal sample
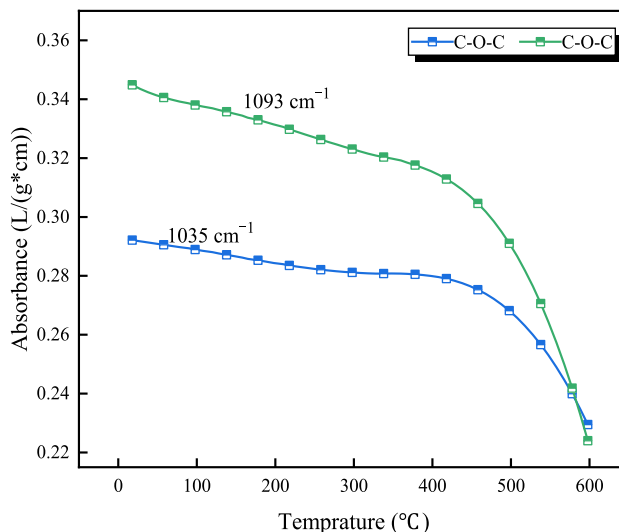
(b) Composite sample

Fig. 10 Curves of oxygen-containing functional groups with temperature for **a** Raw coal sample and **b** Composite sample

the high-temperature combustion stage, because of the later reaction, free hydroxyl groups and intramolecular hydrogen bonds, as well as the continuous reaction between the final oxygen-containing functional groups and water, the adsorption strengths of the two types of coal samples were 3690, 3650, and 3620 cm^{-1}, respectively.

In the low-temperature oxidation stage, the absorbance of the methyl deformation vibration of the raw coal sample gradually decreased. While in the mixed sample, the light absorption intensity of the methyl asymmetric expansion

vibration tended to stabilize and rise slightly. Fatty hydrocarbon in samples generally existed in the form of long bonds, general chain bond long activity performance was higher. In low-temperature oxidation stage, as the temperature increased, fatty hydrocarbon attacked by oxygen, fractured into more fatty hydrocarbon, methyl was oxidized, generating CO, CO_2, and hydrocarbon gas. When methyl and methylene production was greater than the consumption absorbance rising, otherwise downward trending. In the stage of rapid heating, the absorbance of the methyl deformation
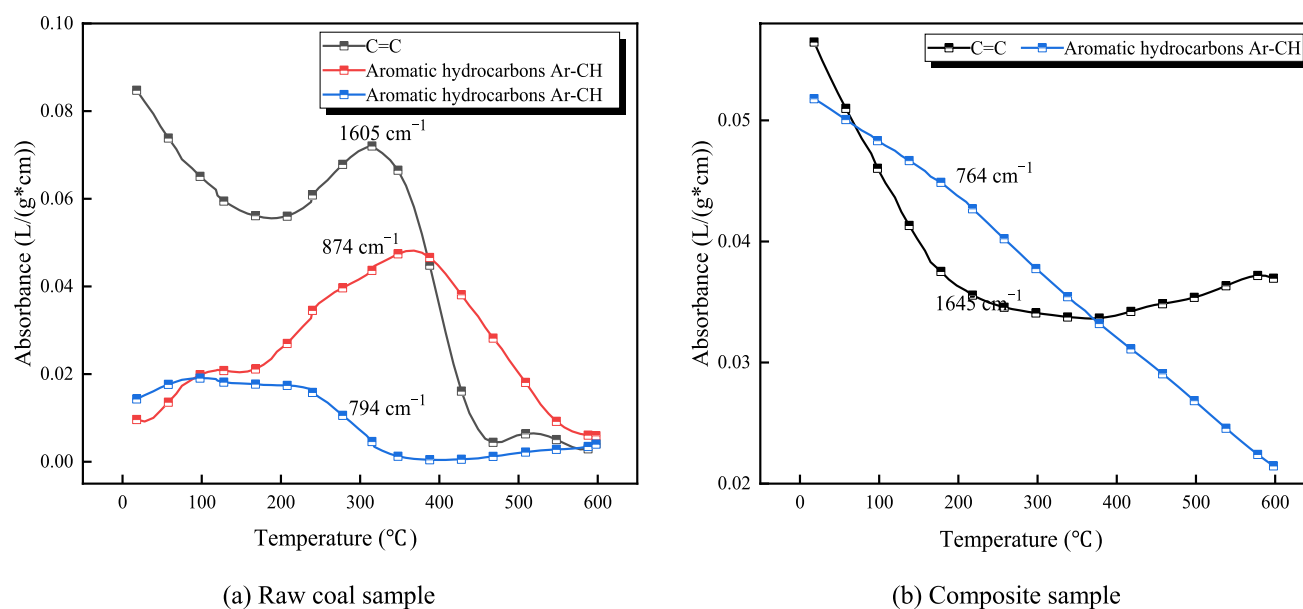
Fig. 11 Curves of aromatic hydrocarbons with temperature for **a** Raw coal sample and **b** Composite sample

vibration of raw coal samples showed a downward trend, while the methyl deformation vibration of mixed samples showed a horizontal trend, with a slightly downward trend.

With the rise of temperature, side chain and oxygen composite generated more CO and water vapor precipitation, leading to reducing fat hydrocarbon side chain, light adsorption intensity reduced high-temperature combustion stage. In raw coal, methylene asymmetric vibration methyl symmetry vibration methyl deformation vibration absorbance dropped swiftly, then fluctuation absorbance increased, then reduced. In the composite sample, the methyl asymmetric expansion vibration commenced to maintain a relatively stable trend, and then started to decline quickly, while the absorbance of the methyl deformation vibration appeared to rise with the temperature, and decreased expeditiously after reaching the peak absorbance. When the 600 °C value was reached, the intensity of methylene asymmetry was already less than 0.1. While the intensity of methyl deformation vibration was slightly greater than 0.1. This indicated that during the oxidation process, the adipose hydrocarbon of the expansion vibration peak was mainly consumed, and that the methylene consumption was greater than the methyl group.

Oxygen-containing functional groups accounted for a large proportion in the total functional groups, and the more active functional groups mainly included carboxyl hydroxyl ether bond fat ether. The main spectrum of the infrared spectrum was fat ether expansion vibration C–O–C, mainly manifested by the wave number of 1093 and 1032 cm^{-1}, in which the coal contains additional phenolic alcohol ether C–O characteristic absorption peak, mainly manifested for aprox. 1263 cm^{-1}.

In the low-temperature oxidation stage, in the raw coal sample, the expansion and vibration absorbance of fat ether with a wavenumber of about 1032 cm^{-1} basically showed an upward trend, while the absorbent intensity of C–O showed an upward trend, while the absorbent intensity of fat ether at about 1083 cm^{-1} had a downward trend. In the mixed samples, the adsorption intensity of the fat ether exhibited a decreasing trend. The light absorption intensity of the fat ether was due to the secondary group containing C–O–C in the oxidation process, which caused the absorbance to rise. In the rapid heating stage for in the raw coal sample, the light absorption intensity of the fat ether expansion vibration bond increased, while the absorbance of C–O also showed an upward trend. In the composite sample mixture, the absorption intensity of the fat ether showed a downward trend. In the high-temperature combustion stage, in the raw coal sample and composite sample mixture, the light adsorption intensity of the fat ether showed a downward trend. In the raw coal sample, the absorbance of C–O also became downward.

In the low-temperature oxidation stage, the vibration absorbance of the deformation of about 1605 cm^{-1} and the deformation of 794 cm^{-1} was decreasing, and the absorbance of the deformation of the substituted aromatics around 871 cm^{-1} was rising. The vibration absorbance of C=C double bonds and various substituted aromatics in the composite sample mixture was decreasing. The C=C double bond was related to the oxidation reaction of the fat hydrocarbon side chain. Because of the participation of the fat hydrocarbon side chain in the oxidation reaction, which led to the decrease of its content, the aromatic ring structure of various

substituted aromatic hydrocarbons began to react and then consume. At this time, the consumption was greater than the production amount, resulting in a downward trend. In the rapid heating stage for in the raw coal sample, the vibration absorbance of C=C double bond with wave number of about 1605 cm^{-1} and wave number of about 871 cm^{-1} kept rising, and the vibration absorbance of a deformation of substituted aromatics of rough 794 cm^{-1} was decreasing. In the composite sample mixture, the absorbance of C=C began to decrease, and the vibration absorbance of various substituted aromatics continued to decrease.

The generation and consumption of C=C double bonds were almost equal, so the absorbance remained constant, exceeding the production amount with increasing temperature, resulting in a decreasing curve. In the high-temperature combustion stage, in the composite sample of raw coal samples, the vibration absorbance of various substituted aromatics with wave number of roughly 1605 cm^{-1} and wavenumber of approximately 794 cm^{-1} was decreasing. In the raw coal sample, the vibration absorbance of deformation of various substituted aromatics with wave number of ca. 794 cm^{-1} decreased. In the composite sample mixture, the C=C double bond wave number and the vibration absorbance of various substituted aromatic hydrocarbons showed a decreasing trend. Owing to the increasing temperature, the stable functional group structure fractured, producing a large number of substituted hydrocarbon group. Meanwhile, the absorbance slightly exhibited an upward trend, while the deformation vibration of a variety of substituted aromatic hydrocarbons still decreased with the continuous reaction.

3.4 Analysis of the pit mineral dynamics

The data of the main functional groups analyzed by in–situ infrared spectroscopy were evaluated by Achar differential method and Coats-Redfern integral method.

(1) The Coats-Redfern integration method.

Coats-Redfern is a method for calculating kinetic parameters based on the results of heating rate test.

$$\ln \frac{g(\alpha)}{T^2} = -\frac{E_a}{RT} + \ln \left[\frac{AR}{\beta E_a} \right] \tag{3}$$

In Eq. (3), the conversion degree (α) of coal at time T; T is the temperature, K; also E_a is the apparent activation energy, kJ/mol; R is the universal gas constant, $R = 8.314$ J/(mol·K); A refers to the prefactor, S^{-1}; β is the heating rate, K/min. 1000/T using ln (g (α)/T^2) to obtain the apparent activation energy E_a.

$$E_a = -KR \tag{4}$$

(2) Achar differentiation

$$\ln \frac{d\alpha}{f(\alpha)dT} = \ln \frac{A}{\beta} - \frac{E_a}{RT} \tag{5}$$

In Eq. (5), when the heating rate of β is certain, map 1000/T with ln[dα/dT/$f(\alpha)$], and then make a linear fitting, and obtain the apparent activation energy E_a from the slope of the resulting quasi-t line.

The light absorption intensity of the functional group was used to calculate the conversion degree.

$$A = \frac{(A_n - A_1)}{(A_n - A_{End})} \tag{6}$$

In Eq. (6), the absorptive intensity of the functional group at the beginning of the initial stage; A_1 is the absorption intensity of the functional group at time T; A_{End} is the absorptive intensity of the functional group at the end of the stage.

The original data and the commonly used gas–solid reaction mechanism function $f(\alpha)$ and $g(\alpha)$ put into the integral Eqs. (3) and (5), a series of apparent activation energy is properly selected (Zhao et al. 2023). If reasonable $f(\alpha)$ and $g(\alpha)$ can reflect the real reaction, the apparent activation energy is similar, and the correlation coefficient of the fitting curve is excellent. Therefore, similar apparent activation energy and high correlation of a set of mechanism functions were chosen as the most universal mechanism function in this stage.

The hydrogen bond of the association of shear vibration methyl shear in aromatic ring C=C stretching vibration C–O, C–O–C aromatic hydrocarbon Ar–CH, respectively, solved the mechanism function of different oxidation stages, selected the highest fit as the reactions apparent activation energy, and took the free hydroxyl group in composite sample as an example. The integration method and differential method of different mechanism functions of the apparent activation energy and fit degree are summarized in Figs. 12, 13, and 14.

From the data in Figs. 12, 13 and 14, it can be clearly observed that the free hydroxyl group in the hydroxyl group of the mixed sample adopted the 2D diffusion Valensi equation of the integral method during the low-temperature oxidation stage. The fitting coefficient R^2 reached the maximum value, e.g., 0.999. That is, the diffusion model best reflected the apparent activation energy of the functional groups during the reaction. By the Avrami-Erofeev equation ($n = 4$), the fitting coefficient R^2 reached the maximum value, e.g., 0.984. That is, the random nucleation and growth models can best reflect the apparent activation energy of the functional groups during the reaction. The one-dimensional
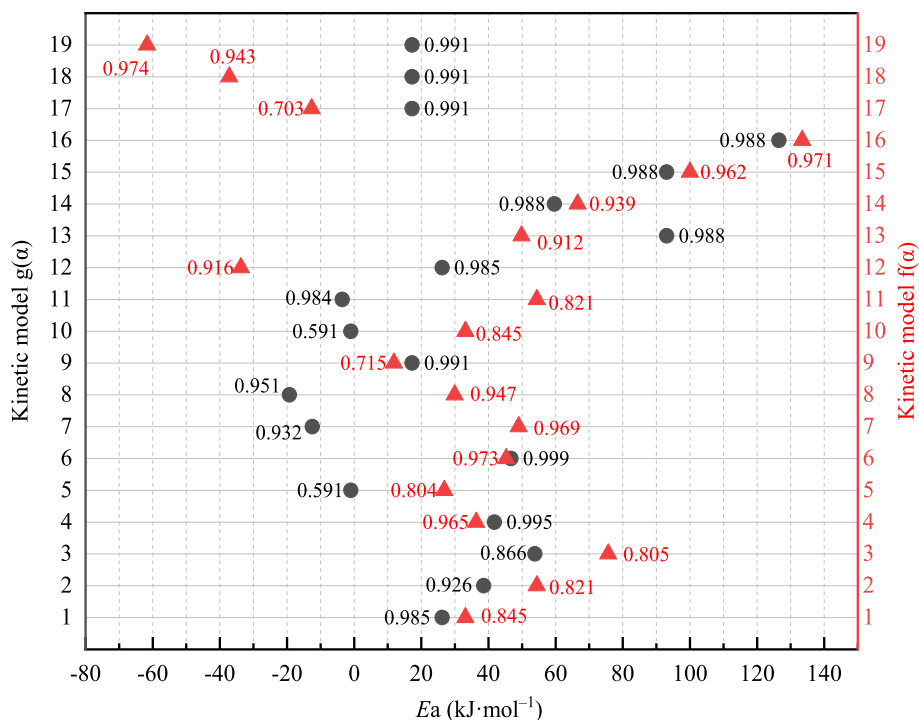
Fig. 12 Mechanism functions of the four mixed free hydroxyl groups are solved during the low-temperature oxidation phase
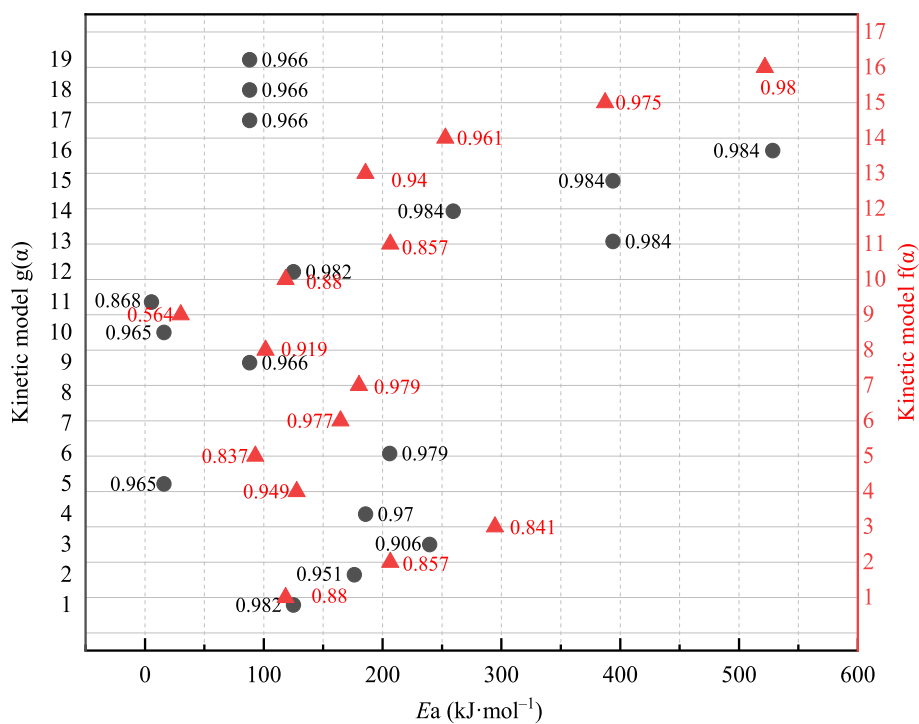
Fig. 13 Mechanism functions of the four mixed free hydroxyl groups during the rapid heating phase
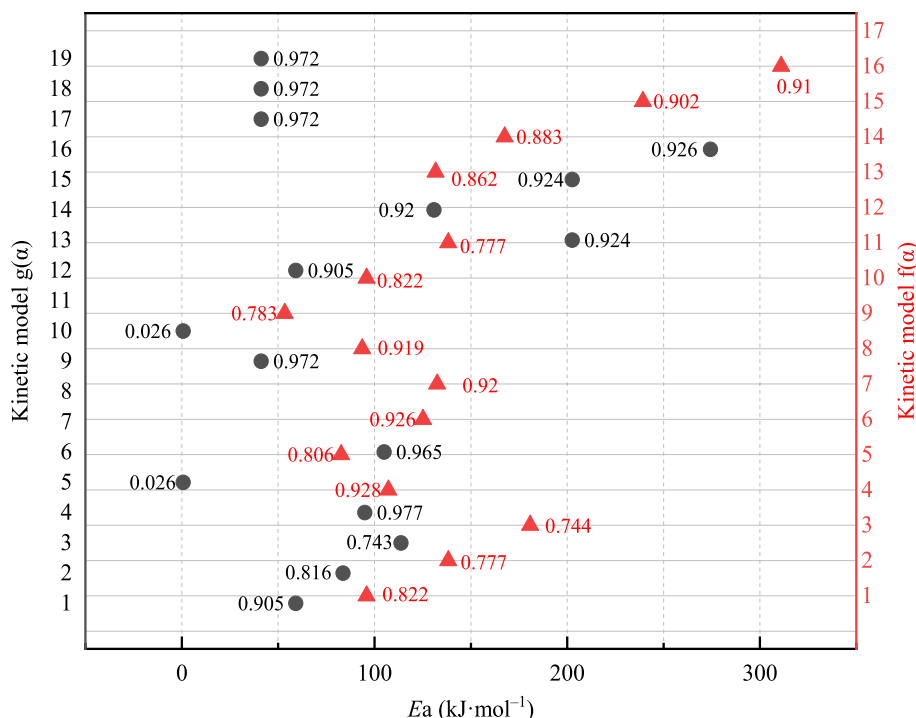
Fig. 14 The mechanism functions of the four mixed free hydroxyl groups during the high-temperature combustion phase

diffusion parabolic rule of the integral method was adopted in the high-temperature combustion phase. The fitting coefficient R^2 reached the maximum value, for instance, 0.977. As planned, the results showed that the diffusion model best reflected the apparent activation energy of the functional groups during the reaction for the remaining active functional groups. This study took the same approach. The apparent activation energy was calculated by integral and differential methods, by selecting the most highly fitted reaction model as the mechanism function. Using this apparent activation energy as the basis for the subsequent analysis, the apparent activation energies of each functional group at different stages are shown in Fig. 11.

As can be seen from Fig. 15, the E_a of the functional groups in the raw coal and the composite samples were small in the low-temperature oxidation stage, indicating that the functional activity of the two samples was high in this stage, the low-temperature oxidation stage was 0–220 °C, the rapid heating stage was 220–580 °C, and the high-temperature combustion stage was more than 580 °C. Mixed samples of hydroxyl fatty hydrocarbon oxygen functional group of three types of groups apparent activation energy were substantially higher than raw coal. This was because in the process of coal oxygen composite reaction, as the temperature rose, adsorption on the sample surface of oxygen molecules and oxygen functional groups, such as carboxyphenolic hydroxyl

oxygen atoms slowly decomposed. At the same time, the organic matter in oil shale root for shale oil, combined with four mixed with coal gangue, exacerbated the difficulty of the chemical reaction; the energy increased, the comprehensive influence of various factors eventually led to its apparent activation energy which was higher than raw coal. Because of the small quartz mineral content in raw coal, the less fatty hydrocarbon structure, inter-molecular aromatic ring layer stack height was small. The loose microcrystalline structure, aliphatic structure content, aromatic ring condensation degree, and layer structure were relatively orderly. Here, a variety of conditions in the chemical reaction played a vital role in promoting, and mixing the sample of high quartz content and raw coal; on the other hand, the apparent activation energy of aromatic coal was greater than composited.

4 Conclusions

The oxidation dynamics of open-pit minerals were studied from both microscopic and macroscopic perspectives. Combined with pore characteristics and exothermic characteristics, the oxidation stage of coal spontaneous combustion process was divided, and the migration and conversion rules of functional groups with temperature were analyzed. In summary, the following conclusions were obtained:

(a) E_a of hydroxyl

(b) E_a of adipose hydrocarbon

(c) E_a of oxygen-containing functional groups

(d) E_a of aromatic hydrocarbon
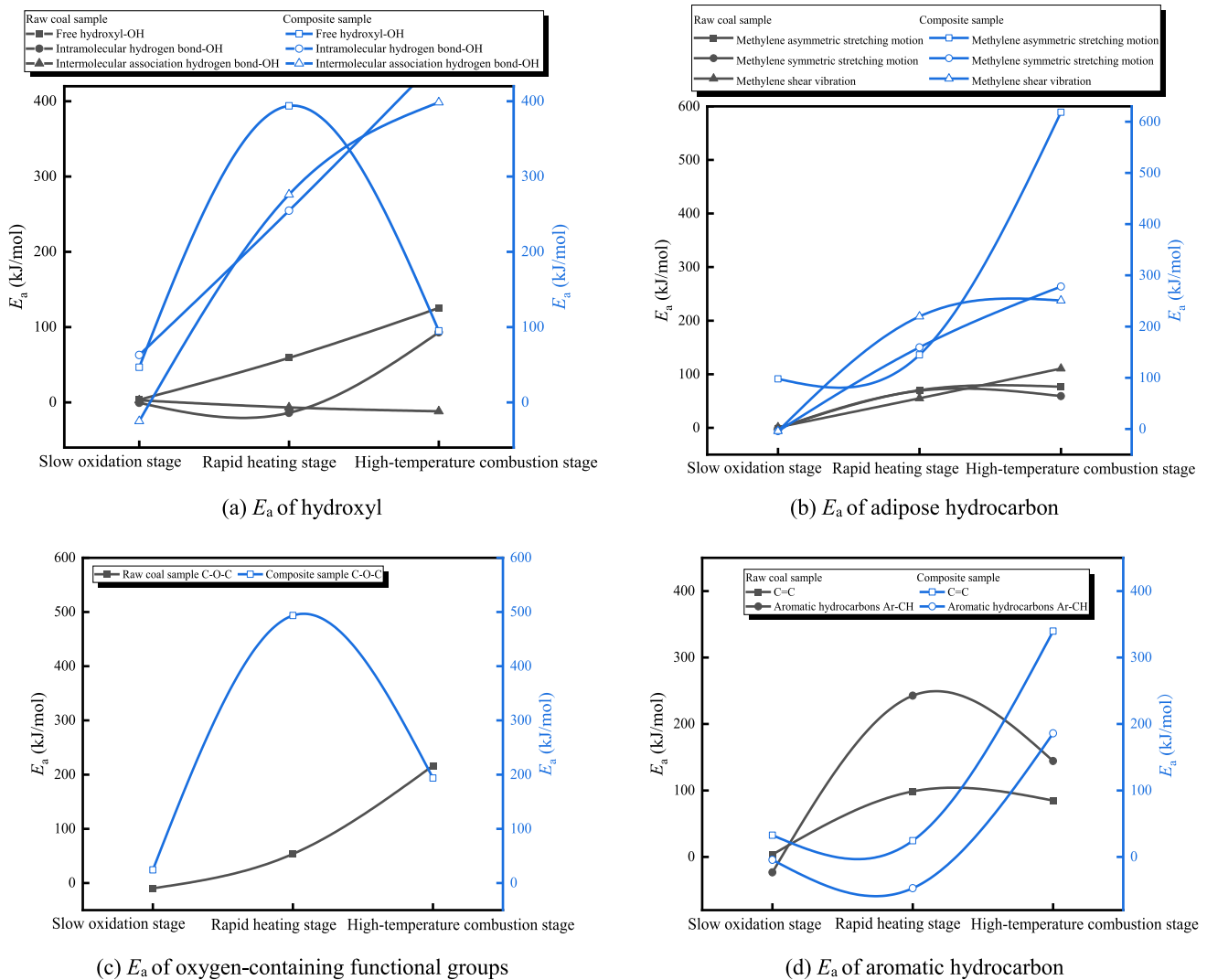
Fig. 15 E_a of different functional groups of raw coal mixed with composite samples

(1) The raw coal sample possessed high fixed carbon content. After the composite samples were affected by coal gangue, the fixed ash content was high, the element content decreased with temperature, and the specific surface area was abated. The large aperture distribution was slightly higher than that of the middle pore, the micropore was exceedingly low, and the gas adsorption capacity was weaker than that of raw coal. The oxygen channels of raw coal were more than the composite samples, and the heat storage capacity was weaker than the composite samples.

(2) Using DSC curve, two samples of combustion process were divided into low-temperature oxidation, expeditious heating and high-temperature combustion with three stages of raw coal sample of DSC curve and heat. The surface of the coal active functional group was more likely to react with oxygen. However, compos-

ite samples after mixing DSC curve possessed similar trend. With the rising temperature, the DSC curve increased in the downward trend. This was due to the active functional group in the sample of a large number of small molecular structures and oxygen reaction. The sample released an enormous amount of heat, then the DSC curve began to rise.

(3) The free hydroxyl group and inter-molecule hydrogen bonds appeared in the inter-molecular hydrogen bond. However, the methyl light absorption intensity was higher than the other samples. The highest absorbance of the C–O–C functional groups contained in the mixed samples was found in the oxidation process. The free hydrogen bond –OH in the mixed samples demonstrated a trend of first rising and then decreasing. The intensity of the inter-molecular association hydrogen

bond –OH was mainly due to the influence of the alkyl side chain of the sample.

(4) The apparent activation energy of the main active functional groups in raw coal and composite samples exhibited a trend from low to high with the development of oxidation stage, the composite sample increased the main functional group reaction's apparent activation energy, improved the coal activity in low-temperature oxidation phase, and made the less need of heat for oxidation reaction.

Declarations

Competing interests The authors declare that we do not have any commercial or associative interest that represents a conflict of interest in connection with the work submitted.

References

Aich S, Nandi BK, Bhattacharya S (2019) Effect of weathering on physico-chemical properties and combustion behavior of an Indian thermal coal. Int J Coal Sci Technol 6:51–62

Alexander VB, Yuan CD, Mikhail AV et al (2023) In-situ combustion technique for developing fractured low permeable oil shale: experimental evidence for synthetic oil generation and successful propagation of combustion front. Fuel 344:127995

Cao DY, Wang AM, Ning SZ et al (2020) Correction to: coalfield structure and structural controls on coal in China. Int J Coal Sci Technol 7:417

Chabukdhara M, Singh OP (2016) Coal mining in northeast India: an overview of environmental issues and treatment approaches. Int J Coal Sci Technol 3:87–96

Deng J, Ma XF, Zhang YT et al (2015) Effects of pyrite on the spontaneous combustion of coal. Int J Coal Sci Technol 2:306–311

Huang XD, Kang ZQ, Zhao J et al (2023) Experimental investigation on micro-fracture evolution and fracture permeability of oil shale heated by water vapor. Energy 277:127677

Jiang HY, Liu S, Wang J et al (2023) Study on evolution mechanism of the pyrolysis of chang 7 oil shale from Ordos basin in China. Energy 272:127097

Jin JF, Sun JS, Lü KH et al (2023) Catalytic pyrolysis of oil shale using tailored Cu@zeolite catalyst and molecular dynamic simulation. Energy 278:127858

Ju Y, Zhu Y, Xie HP et al (2019) Fluidized mining and in-situ transformation of deep underground coal resources: a novel approach to ensuring safe, environmentally friendly, low-carbon, and clean utilisation. Int J Coal Sci Technol 6:184–196

Liang YT, Yang YL, Guo SD et al (2023) Combustion mechanism and control approaches of underground coal fires: a review. Int J Coal Sci Technol 10:24

Liu YM, Xue LF, Ma JX et al (2023) Three-dimensional numerical simulation, energy efficiency and economic benefit estimation of oil shale in situ pyrolysis process. Geoenergy Sci Eng 227:211804

Onifade M, Genc B (2019) Spontaneous combustion liability of coal and coal-shale: a review of prediction methods. Int J Coal Sci Technol 6:151–168

Tang YG (2020) Special issue on coal geology in China. Int J Coal Sci Technol 7:217–219

Tang YG, Li RQ, Wang SQ (2020) Research progress and prospects of coal petrology and coal quality in China. Int J Coal Sci Technol 7:273–287

Wang XM, Wang Q, Pan S et al (2023) The non-isothermal thermal decomposition evolution of the Fushun oil shale kerogen based on ReaxFF molecular dynamics simulation. J Analy Appl Pyroly 169:105869

Zeng Q, Li S (2022) Experimental study on the oxidation kinetics of coal in typical coal mining areas of the Southern Junggar coalfield, Xinjiang, China. Int J Coal Sci Technol 9:78

Zhai YM, Yang TH, Zhang Y et al (2023) Co-pyrolysis characteristics of raw/torrefied corn stalk and oil shale. J Analy Appl Pyrol 171:105967

Zhang L, Qi SC, Takeda N et al (2018) Characteristics of gas evolution profiles during coal pyrolysis and its relation with the variation of functional groups. Int J Coal Sci Technol 5:452–463

Zhang LJ, Zhou X, Zhou Y et al (2022) Surface coal mining impacts on land use change and ecological service value: a case study in Shengli coalfield, Inner Mongolia. Int J Coal Sci Technol 9:65

Zhao JY, Ming HQ, Guo T et al (2022) Semi-enclosed experimental system for coal spontaneous combustion for determining regional distribution of high-temperature zone of coal fire. Int J Coal Sci Technol 9:62

Zhao JY, Xiao YY, Song JJ et al (2023) Kinetic properties of non-caking coal spontaneous combustion by evolution of its functional groups. Fuel 354:129428

Zheng Y, Lei GL, Yao CJ et al (2023) Characteristics and kinetics of Maoming oil shale pyrolysis in the presence of $CoCl_2$ assisted steam. Fuel 338:127279

Zhu T, Wang RN, Yi NJ et al (2020) CO_2 and SO_2 emission characteristics of the whole process industry chain of coal processing and utilization in China. Int J Coal Sci Technol 7:19–25

Publisher's Note Springer Nature remains neutral with regard to jurisdictional claims in published maps and institutional affiliations.